Observation of Excitonic Fine Structure in a 2D Transition-Metal Dichalcogenide Semiconductor

Jingzhi Shang,[†] Xiaonan Shen,[†] Chunxiao Cong,[†] Namphung Peimyoo,[†] Bingchen Cao,[†] Mustafa Eginligil,[†] and Ting Yu[*,†,‡,§]

[†]Division of Physics and Applied Physics, School of Physical and Mathematical Sciences, Nanyang Technological University, Singapore 637371, [‡]Department of Physics, Faculty of Science, National University of Singapore, Singapore 117542, and [§]Graphene Research Centre, National University of Singapore, 2 Science Drive 3, Singapore 117542

ABSTRACT Two-dimensional (2D) semiconductors, such as transition-metal dichalcogenide monolayers (TMD 1Ls), have attracted increasing attention owing to the underlying fundamental physics (*e.g.*, many body effects) and the promising optoelectronic applications such as light-emitting diodes. Though much progress has been made, intrinsic excitonic states of TMD 1Ls are still highly debated in theory, which thirsts for direct experimental determination. Here, we report unconventional emission and excitonic fine structure in 1L WS_2 revealed by electrical doping and photoexcitation, which reflects the interplay of exciton, trion, and other excitonic states. Tunable excitonic emission has been realized in a controllable manner *via* electrical and/or optical injection of charge carriers. Remarkably enough, the superlinear (*i.e.*, quadratic) emission is unambiguously observed which is attributed to biexciton states, indicating the strong Coulomb interactions in such a 2D material. In a nearly neutral 1L WS_2, trions and biexcitons possess large binding energies of ~10−15 and 45 meV, respectively. Moreover, our finding of electrically induced robust emission opens up a possibility to boost the luminous efficiency of emerging 1L TMD light emitting diodes.

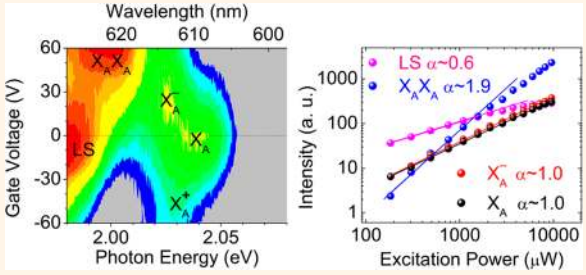

KEYWORDS: two-dimensional semiconductor · transition-metal dichalcogenide · photoluminescence · trion · biexciton

Atomically thin transition-metal dichalcogenides (TMDs) have aroused great attention because of their intriguing physical properties and promising optoelectronic applications.[1−3] In particular, monolayers (1Ls) of MoS_2, $MoSe_2$, WS_2, and WSe_2 as a group of direct-band two-dimensional (2D) semiconductors provide a new platform to realize electronic and optical functionalities in ultrathin, flexible, and/or transparent devices, such as transistors[4,5] and light-emitting diodes,[6−8] which could potentially be superior alternatives of conventional Si and III−V based semiconductors. Distinct from the conventional bulk and quasi-2D semiconducting materials, quantum confinement and reduced dielectric screening in 2D semiconductors enhance quasiparticle interactions and result in large binding energies of excitons and trions,[9−13] where many-body effects need to be taken into account for the electronic and excitonic band structures. The compelling optical properties of TMD 1Ls are strongly correlated to their quasiparticle band structures and significantly influenced by the large excitonic effects.[14,15]

Due to the existence of quantum confinement and large excitonic effects in 2D semiconductors, investigations of many-body physics become a very exciting research field for exploring fundamentals of quantum mechanics. In particular, the information on elementary excitations is essential to study many-body interactions. Precise determination of basic quantities of binding energies is critical for clarifying the current theoretical debate on quasiparticle band structures of 1L TMDs.[14,15] Through experimental probes such as scanning tunnelling spectroscopy (STS), temperature-dependent photoluminescence (PL) and/or nonlinear optical spectroscopy, the binding energies of A excitons in 1L MoS_2,[16] $MoSe_2$,[17] WSe_2[18] and WS_2[19−22] were measured to be in a

* Address correspondence to yuting@ntu.edu.sg.

Received for review October 21, 2014 and accepted January 5, 2015.

Published online 10.1021/nn5059908

range of 0.2 to 0.8 eV. However, the exact values are still under discussion probably due to the spectral overlapping of near-band-edge electronic and excitonic transitions. In nearly neutral 1Ls of MoS_2,[9] $MoSe_2$,[23] and WSe_2,[24] the binding energies (18−30 meV) of trions were uncovered. For 1L WS_2, the binding energy of negative trions is still controversial,[19,20,25] and the information on the positive trions is less known. In addition to the exciton and trion states confirmed by the previous studies,[9,23,24] for 2D semiconductors of high quality, formation of biexciton is highly expected and desired owing to its unique roles in understanding many-body effects and developing practical applications. Though the excited-state absorption features have been correlated to the biexciton formation in 1L MoS_2,[26] the direct observation of biexciton emission in TMD 1Ls is still highly desired.

The excitonic emission and the dissociation energies of trions in TMD 1Ls have been found to be sensitive to the electrical doping[9,23,24] and photoexcitation.[25] These studies have been focused on electrical or photoinduced doping effect independently. By contrast, how the excitonic emission responds to both electrical doping and excitation power simultaneously remains unclear in 1L TMDs, especially for 1L WS_2, a very promising candidate for optoelectronic applications possessing much stronger light emission than 1L MoS_2 and a more favorable emission energy (visible) than 1L Mo/WSe_2 (near-infrared). Exciting enough, the electroluminescence from 1L diodes of MoS_2,[7,27] WSe_2,[6] and WS_2[8] was demonstrated, yet the low efficiency (typically less than 1%) might be a bottleneck for further practical applications. Hence, thoroughly understanding and further modulating the excitonic emission become a basis for solving such issues. In this work, by separately and jointly controlling the electrical doping and the photoexcitation strength, we have observed the intrinsic excitonic states and achieved the tunable emission in 1L WS_2. The roles of unconventional excitonic states are identified in the near-band edge emission of 1L WS_2. The basic quantities of binding energies of both positive and negative trions have been extracted from a nearly neutral 1L WS_2. In particular, the striking biexciton emission is electrically controllable, which promises a bright future of significantly improving luminous efficiency in 1L WS_2 diodes.

RESULTS AND DISCUSSION

Here, all of the PL measurements were performed at the excitation power of 65 μW unless otherwise specified. Figure 1a shows PL spectra from a field effect device of exfoliated 1L-WS_2 taken at the back-gate voltages from −40 to +40 V, which reflect the excitonic emission near the band edge at room temperature (rt). On the whole, the emission band consists of two components, where the high/low energy peak becomes dominant at −40/40 V and is assigned to A exciton (X_A)/negative trion (X_A^-) emission, as seen in Figure 1b. On the one hand, from −40 to +40 V, the peak position of X_A^- apparently redshifts and that of X_A slightly blueshifts (Figure 1c). Consequently, the energy difference of X_A and X_A^- increases, which is strongly related to phase space blocking[28] and many body effects.[29] We define this energy splitting as the dissociation energy of trion, which consists of the trion binding energy (E_{tb}) and the Fermi level (E_f). In a simplified model,[9,30] the dissociation energy of trion is $E_{tb} + E_f$, where E_{tb} is considered to be a constant. The increase of the dissociation energy of trion with electron doping is mainly due to the rising of Fermi level. In case the trion binding energy varies with doping,[28] further theoretical investigation is needed to fully address the observed trend. The exciton energy can be estimated by $E_g - E_{exb}$, where E_g and E_{exb} are the band gap and the exciton binding energy, respectively. The blueshift of exciton energy may be due to the decrease in the exciton binding energy with electron doping or the band gap renormalization. A recent theoretical study[28] supports the former, where the electron doping causes the reduction of phase space due to Pauli exclusion and decreases the exciton binding energy. Meanwhile, the electron doping typically causes the reduction of band gap[29,31,32] and thus tends to decrease the exciton energy. Therefore, the blueshift of exciton energy here is attributed to the decrease in the exciton binding energy with electron doping. On the other hand, the total integrated intensity and that of X_A gradually decrease with the increase in the back-gate voltage, while the intensity of X_A^- increases from −40 to 0 V and then remains stable between 0 and 30 V and slightly decreases after 30 V (Figure 1d). The stable feature has been seen in heavily doped 1L MoS_2,[9] and the intensity changes of X_A^- have been observed in the nearly neutral 1L $MoSe_2$.[23] The different responses of these three devices could be due to the different grades of native doping in the original TMD flakes. Special care should be paid to such a study. Figure 1e shows the PL spectra of the CVD-grown 1L WS_2 at varied back-gate voltages (curves) and the total integrated intensity as a function of gate voltage (dots). The emission band mainly contains one component, and its intensity decreases with more electron doping as seen in Figure 1f. Comparing such gate dependence of intensity with that of X_A shown in Figure 1d, we assign this strong peak to the X_A emission. The general agreement of the peak width (~0.04 eV) of the present band with that of X_A in the exfoliated 1L WS_2 further confirms this assignment (see Figure S1a, Supporting Information). At positive voltages larger than 20 V, the emission profile widens and extends to the lower energies (Figure S1b, Supporting Information). With the increasing electron doping, the presence of the emission component of trions and its redshift are expected as seen in Figure 1a, which take responsibility

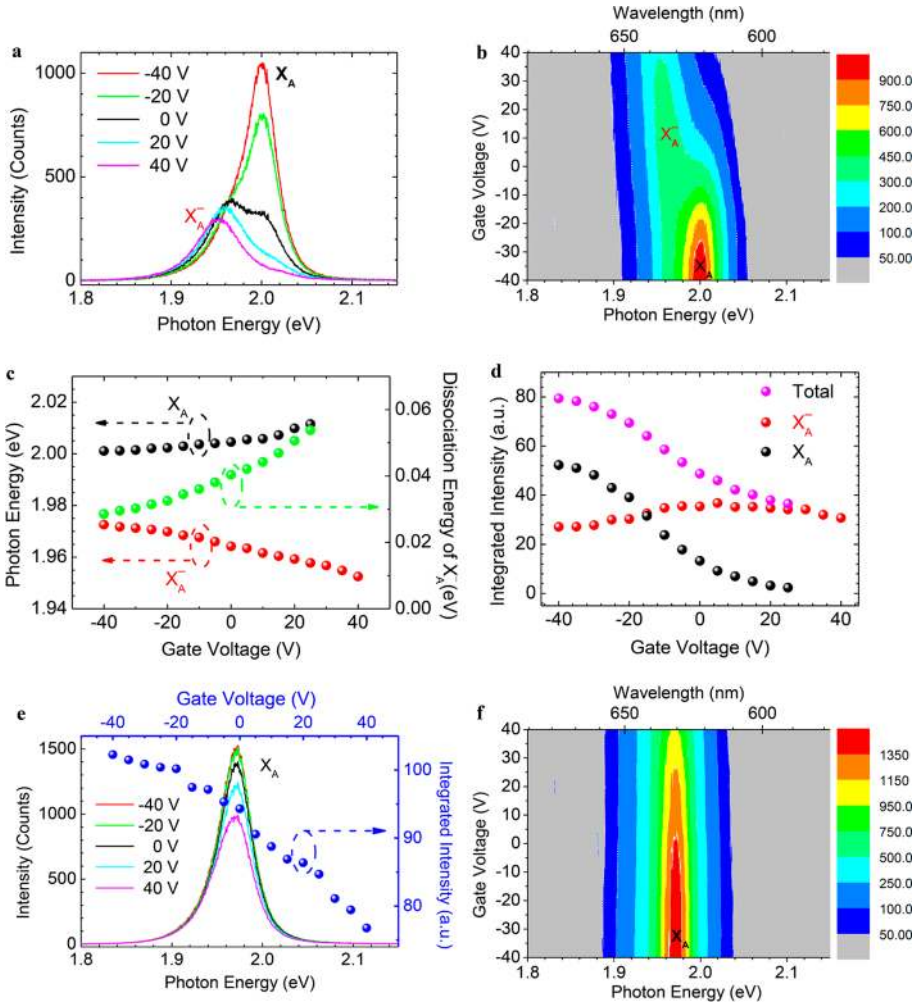

Figure 1. Electrical doping effect on excitonic emission in 1L WS_2 at room temperature. Exfoliated 1L WS_2: (a) Photoluminescence spectra at the back-gate voltages between −40 and +40 V. (b) Photoluminescence intensity mapping as a function of photon energy and gate voltage. (c) Photon energies of A exciton (X_A) and negative trion (X_A^-) (left vertical axis) *versus* gate voltage; dissociation energy of negative trion (X_A^-) (right vertical axis) *versus* gate voltage. (d) Integrated intensities of X_A, X_A^-, and the total emission band *versus* gate voltage. CVD-grown 1L WS_2: (e) Photoluminescence spectra at different back-gate voltages (left vertical axis) and integrated photoluminescence intensity (right vertical axis) *versus* gate voltage (upper horizontal axis). (f) Photoluminescence intensity imaging as a function of photon energy and gate voltage.

for the observed broadening and the low energy tail at 40 V (Figure S1b, Supporting Information).

As noticed in graphene,[33,34] in addition to the electrical doping, the carrier concentration can also be tuned by light illumination. Here, we studied the influence of excitation power on the excitonic emission in 1L WS_2 at both room and cryogenic temperatures and explored the possibility of controlling the excitonic emission optically. Figure 2a shows the representative PL spectra of an exfoliated 1L WS_2 device taken under four excitation powers. The overall emission band profile evolves from the two-component feature at low excitation powers into a single peak at high powers. To further reveal the response of excitons and trions to photoexcitation, their emission energies and strengths are plotted as functions of the excitation power. As shown in Figure 2b, with the increase in the excitation power, the X_A peak blueshifts while the X_A^- peak redshifts; the integrated intensity of X_A^- increases linearly while that of X_A sublinearly increases at lower excitation powers (<1000 μW) and saturates at higher excitation powers (>1000 μW). These peak shifts and the rising intensity ratio of X_A^-/X_A are in line with our electrical doping measurements (see Figure S2, Supporting Information) and are mainly attributed to the photoinduced electron doping, which is further evidenced by the electrical transport measurements under photoexcitation (Figure S3, Supporting Information). In the n-type exfoliated 1L WS_2, at a low temperature (4 K)[25] such photoinduced doping effect has also been observed. Note that the possible lattice heating induced by photoexcitation will cause the redshift of exciton band while the blueshift presents here. It indicates that the laser heating is a minor factor in our cases. Figure 2c shows the PL spectra of the CVD-grown 1L WS_2 at different excitation powers. The peak

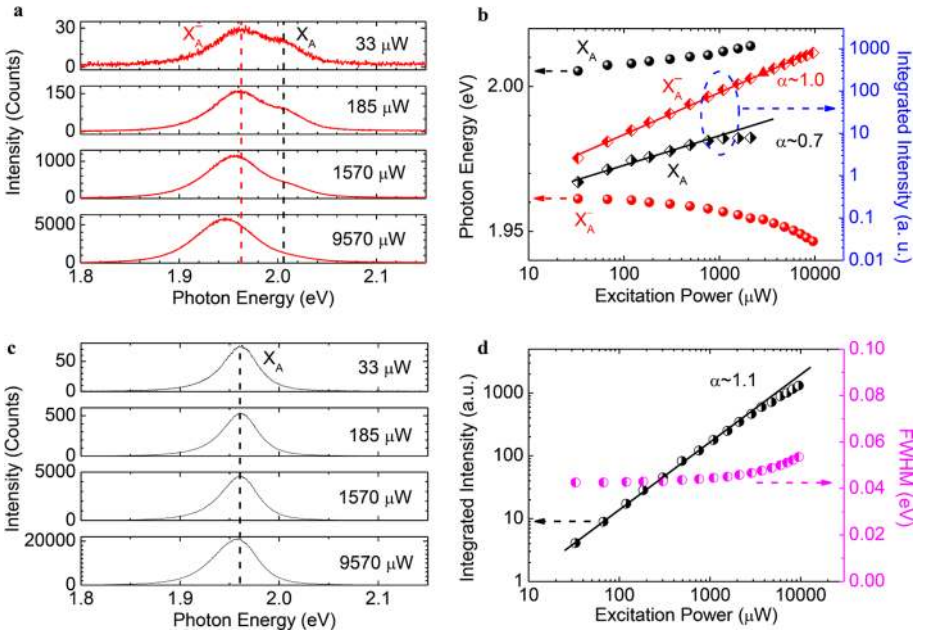

Figure 2. Influence of excitation power on excitonic emission in 1L WS_2 at room temperature. Exfoliated 1L WS_2 field-effect device: (a) Photoluminescence spectra at different excitation powers. (b) Dependences of photon energies and integrated intensities of A exciton and negative trion bands on excitation power. CVD-grown 1L WS_2 field-effect device: (c) Photoluminescence spectra at different excitation powers. (d) Integrated peak intensity and full width at half-maximum (fwhm) as a function of excitation power. Solid lines in b and d are the linear fit curves on log−log scales where the α values represent the slopes.

shape maintains at the first three excitation powers and becomes asymmetric at the highest excitation power. In detail (Figure 2d), the total integrated intensity of PL linearly increases with the excitation power (<2500 μW) and slightly deviates at high excitation powers (>2500 μW). The width of PL is nearly constant at the excitation power less than 2500 μW. At higher excitation powers, the band broadens toward to lower photon energies and becomes more asymmetric, which is analogous to the PL evolution induced by electrical doping (Figure S1b, Supporting Information) and results from the presence of excitonic emission from negative trions induced by strong photoexcitation.

As presented above, the PL spectrum of CVD-grown 1L WS_2 at rt mainly shows one single component of X_A(Figure 1e). When the temperature cools down to a cryogenic temperature of 4.2 K, one broad band appears at the low energies and the other high-energy band becomes asymmetric at the excitation powers of 7 and 65 μW as shown in the upper and middle panels of Figure 3a, respectively. The corresponding emission spectra can be well deconvoluted by three Lorentzian peaks, assigned to X_A, X_A^- and localized states (LS). The LS are probably due to shadow impurities, defects, and/or disorder effects, which deserves further investigation. Similar emission bands with the lower energies than those of exciton and trion states have often been observed in other TMD 1Ls of MoS_2, $MoSe_2$, and WSe_2.[6,23,35−37] At a high excitation power of 9570 μW, the X_A^- peak becomes more obvious and another new band appears (Figure 3a, bottom panel). The new band is assigned to the biexciton emission in 1L WS_2, denoted as X_AX_A, which will be further discussed later. More clearly, the gradual evolution of the emission bands with the excitation power is seen in the PL intensity mapping *versus* excitation power and photon energy (Figure 3b). Figure 3c presents the peak positions of four components as a function of excitation power. As shown in Figure S4 (Supporting Information), the dissociation energies of negative trions are 13−15 meV, which slightly increases with the excitation power due to photoinduced doping; for X_AX_A, the extracted dissociation energies are between 50 and 60 meV. In the electrical transport measurements of the CVD-grown 1L WS_2 device (Figure S5, Supporting Information), the turn-on voltage shifts to negative gate voltages with the increasing excitation power which verifies the increasing electron doping at 4.2 K by photoexcitation. Figure 3d presents the integrated intensities of X_A, X_A^-, X_AX_A, and LS as functions of the excitation power. With the increase in the excitation power, the emission from exciton and trion states linearly increases over the whole studied range. The emission from LS shows a sublinear dependence (<2200 μW, $\alpha \sim 0.6$). The defect-induced emission band in 1L MoS_2 also presents a sublinear behavior,[38] which is consistent with our data. Remarkably, the integrated intensity of X_AX_A grows quadratically with the excitation powers (<2000 μW, $\alpha \sim 1.9$), which is a strong evidence for biexciton emission. Meanwhile, the typical crossover of exciton and biexciton intensities

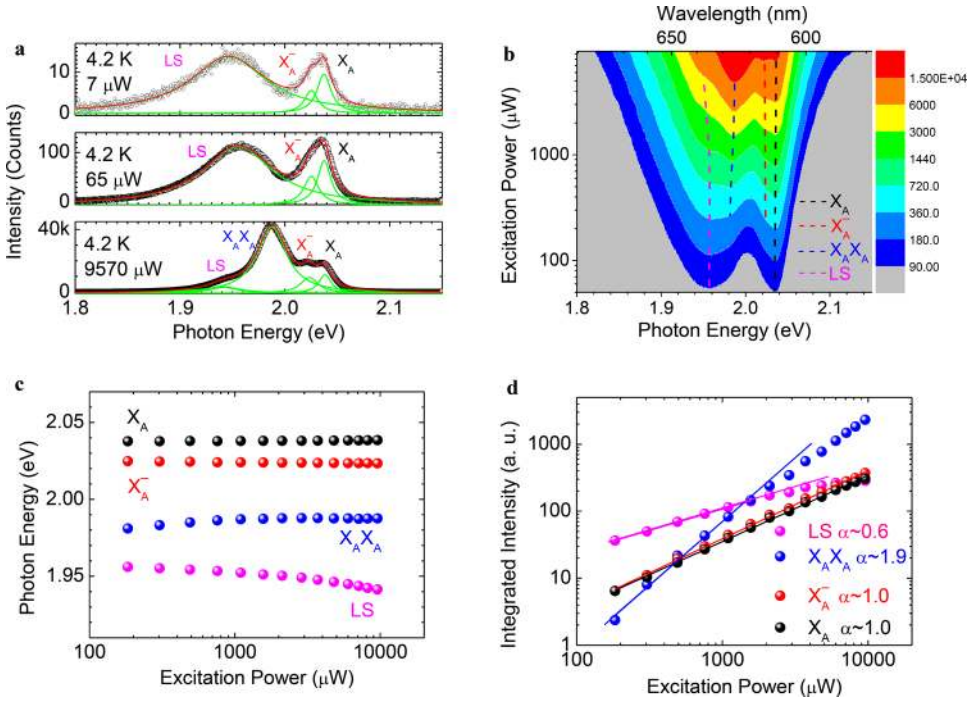

Figure 3. Exciton, trion and biexciton states in a CVD-grown 1L WS_2 at 4.2 K. (a) Photoluminescence spectra at various excitation powers. The total fit curve and subpeaks are shown in red and green, respectively. (b) Photoluminescence intensity mapping *versus* excitation power and photon energy, where dash curves are guide lines to indicate the spectral evolution. (c) Photon energies of four emission components *versus* excitation power. (d) Log−log plots of integrated intensities of four emission components *versus* excitation power. Solid lines are the linear fit curves, and the corresponding α values are the slopes.

has also been observed with the increasing excitation power. Moreover, it is found that the fwhm of the X_AX_A peak is ~2.1 times of that of X_A (Figure S4d, Supporting Information). In ideal cases, the spectral width reflects the quasiparticle decay rate[39−41] and the biexciton lifetime is expected to be half of the exciton lifetime.[42,43] Assuming the homogeneous broadening[39,40] dominating for the observed PL at 4.2 K, the observed width ratio of X_AX_A to X_A (~2.1) could be another signature for the biexciton emission in 1L WS_2. Furthermore, the linear polarization dependences of photon energies of X_A, X_A^-, X_AX_A ,and LS have been measured at three excitation powers (Figure S6, Supporting Information). The sinusoidal modulation has been found for X_A, X_A^- and X_AX_A components, while there are no periodic trends for the LS component. In particular, the opposite linear polarization behaviors of photon energies have been observed for X_A and X_AX_A, which is a unique characteristic for identifying the X_AX_A.[44−47] Theoretically, in 2D case, the binding energy ratio of biexcitons to excitons is ~0.08 according to an exciton basis model[48] when the effective masses of electrons and holes in 1L WS_2 are taken as 0.27 and 0.32,[49] respectively. Recent works have extracted the exciton binding energies of 0.53−0.71 eV for 1L WS_2.[20−22] As a result, the calculated biexciton binding energies of 42−57 meV agree well with our observations above. In addition, in transient absorption measurements of the similar material of 1L MoS_2,[26,50] the photoinduced absorption features have been correlated to biexciton formation, where the extracted binding energies of 70 at 74K[26] and 35 meV at 10 K[50] for the biexcitons of X_AX_A are in the same order as the data for biexcitons here. Note that the previous transient absorption measurements[26,50] mainly imply biexciton formation *via* upward transitions (absorption), while our present steady-state data directly reflect biexciton emission *via* downward transitions between exciton and biexciton states. Both kinds of techniques are parallel but complementary for uncovering biexciton states in 1L TMDs. On the basis of the discussion above, the observed superlinear emission of X_AX_A is attributed to biexciton states in 1L WS_2. Further experimental investigations by transient four-wave mixing and time-resolved fluorescence spectroscopy together with selective polarizations should be very helpful to elucidate the nature of biexciton and possible multiexciton states in such 2D semiconductors.

Finally, the superposition effect of electrical doping and optical excitation has been further studied, and tunable excitonic emission in a 1L WS_2 field-effect device has been demonstrated in a controllable manner. Figure 4a shows the PL spectra of the CVD-grown 1L WS_2 device at different back-gate voltages and the excitation power of 65 μW. At 0 V, there are mainly two broad bands: the higher energy one from the combination of X_A and X_A^- and the other from the LS at lower energies which could be modified during device fabrication[6,23,51] and not the focus here. With the increase of the positive back-gate voltage, the emission

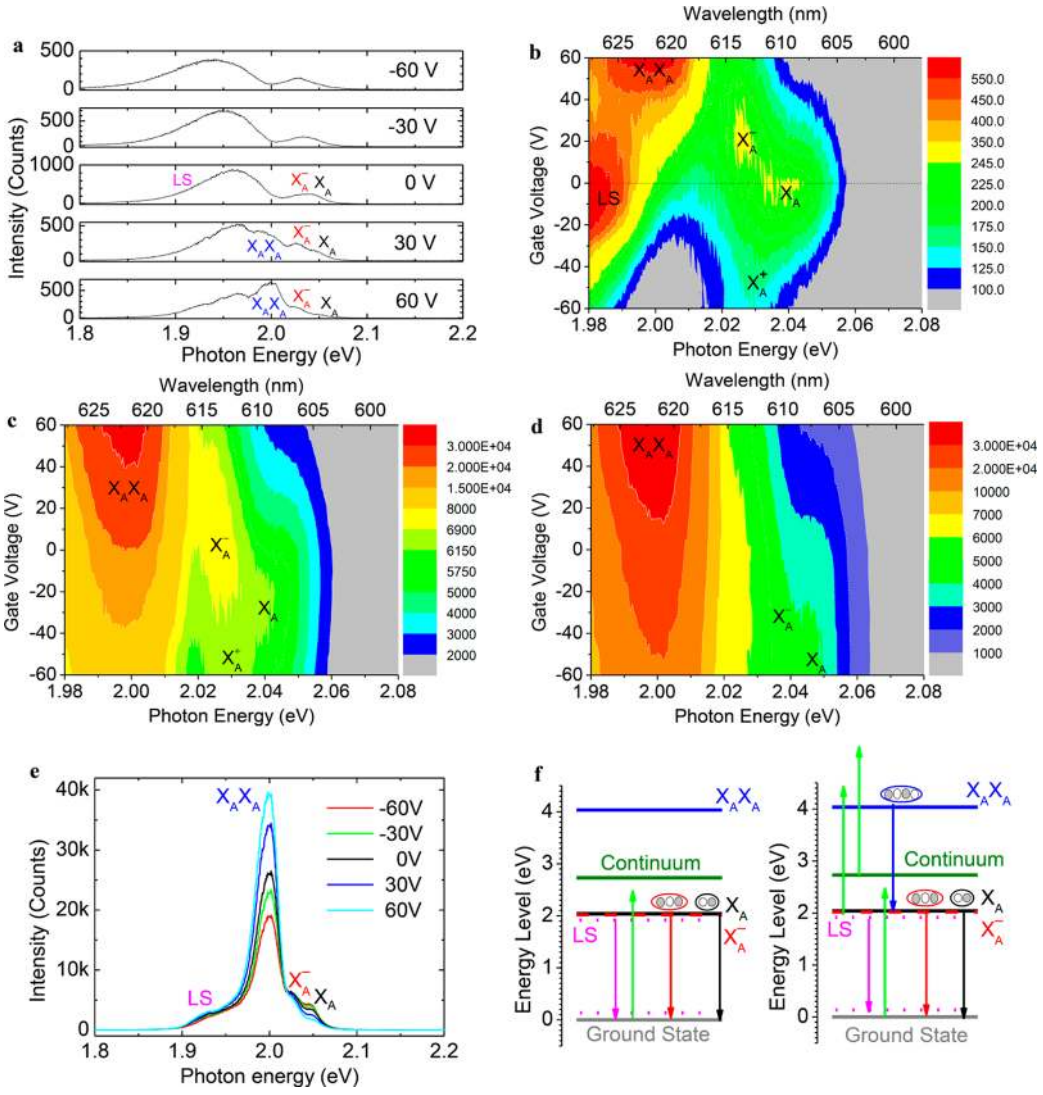

Figure 4. Optoelectronic control of light emission from a single-layer WS_2 field effect device at 4.2 K. (a) Photoluminescence spectra at different gate voltages under the excitation power of 65 μW. (b−d) Photoluminescence intensity mappings *versus* photon energy and gate voltage under the excitation powers of 65, 1570, and 6000 μW, respectively. (e) Photoluminescence spectra at different gate voltages under the excitation power of 6000 μW. (f) Schematics of excitonic and electronic transitions at low (left) and high (right) excitation powers.

from negative trion and biexcion states becomes more obvious. At negative voltages, the enlarged spectra of the higher energy band have been shown in Figure S7 (Supporting Information), which consist of the emission from exciton (X_A) and positive trion states labeled by X_A^+. The evolution of emission states is clearly observed in the PL intensity mapping as a function of photon energy and gate voltage (Figure 4b). The center of exciton emission locates near zero or a small negative gate voltage, which indicates that the sample is nearly neutral or slightly n-doped. The emission zones of positive and negative trions behave like two wings, spreading from the exciton emission center, redshift with the carrier injection. The similar features of trion and exciton bands have been observed in the field effect devices based on 1Ls of WSe_2 and $MoSe_2$.[23,24] More importantly, the X_AX_A emission comes to be pronounced at positive back-gate voltages. As shown in the gate-tuned PL intensity maps at higher excitation powers (Figure 4c,d), the overall feature shifts down with respect to that in Figure 4b due to induced electron doping by strong photoexcitation. In a nearly neutral state of 1L WS_2, the binding energies of ~12, 10, and 45 meV are extracted for negative (X_A^-), positive trions (X_A^+) and biexcitons (X_AX_A), respectively. Note that, on the one hand, the binding energies of trions are much smaller than the thermal energy at rt (k_BT = 26 meV, k_B is the Boltzmann constant); thus, the trion is instable in such a nearly neutral 1L WS_2 at rt which will be thermally activated to lose one electron or hole and form one exciton. This is supported by the almost absence of trion emission in the nearly neutral CVD-grown 1L WS_2 at rt (Figure 1e). On the other hand, the biexciton emission with a binding

energy of ~45 meV is observed at 4.2 K but vanished at rt. This is explained as follows: At 4.2 K, the excited exciton state absorption in the spectral range of biexciton transitions is dominant which is in favor of biexciton formation. This scene is consistent with the recent studies on biexciton formation in 1L MoS_2 at 10 K.[50] At rt, the exciton decay becomes faster than those at low temperatures so that the excited states of biexcitons are hardly formed, and thus, the biexciton emission is absent. The accelerated exciton relaxation has been observed with the lifted temperature in 1L WS_2,[52] which is in line with the explanation above. Figure 4e shows the gate-tuned PL spectra at the high excitation power of 6000 μW, where the X_AX_A emission is dominant and sensitive to the modulated back-gate voltage. Figure 4f shows the schematics of the electronic and excitonic transitions at low (*e.g.*, 65 μW) and high excitation powers (*e.g.*, 6000 μW). Theoretical calculations[14] and recent experiments[19−21] have shown that the electronic band gap of 1L WS_2 is larger than 2.4 eV. Under our laser excitation energy of 2.33 eV, the electrons are pumped up to the lower excitonic levels rather than the continuum. At rt and a low excitation power, the dominant emission is due to exciton states in a nearly neutral sample, both exciton and trion states for a moderate doped sample and trion states for a heavily doped sample, where the trion emission becomes more important at high excitation powers. At a low temperature of 4.2 K, the preferred emission is through exciton, trion and localized states at a low excitation power. The high excitation power and the excited exciton state absorption will cause the photon-induced n-doping and formation of biexciton states. With the increase in the electron doping and the excitation power, the X_AX_A emission starts to be dominant over the other three emission channels by exciton, trion, and localized states.

CONCLUSIONS

In summary, we have studied the intrinsic excitonic emission of a 2D semiconductor 1L-WS_2. By applying the electrical back-gate and varying the excitation power, tunable emission from exciton, trion, biexciton, and localized states has been obtained. At rt, the roles of excitons and trions in PL emission are clearly identified under electrical doping and photoexcitation. At 4.2 K, the emission from localized states appears. With the increase in electron doping and/or excitation power, the superlinear (*i.e.*, quadratic) emission due to biexcitons occurs and becomes dominant. In a nearly neutral 1L WS_2, the binding energies of ~10−15 meV have been extracted for positive and negative trions. Here, the observed biexciton emission in 1L WS_2 reflects strong electron−hole interactions in single-layer semiconductor, which is calling more attention to the research of many-body physics in atomically thin TMD layers. Our studies also develop an efficient strategy for manipulating the excitonic emission, which is valuable to 2D light-emitting applications.

METHODS

Two kinds of 1L WS_2 samples were used here: one was mechanically exfoliated from a synthesized WS_2 crystal (2D semiconductors Inc.) onto SiO_2 (300 nm)/Si (500 μm, p^{+2}) substrates; the other was directly grown on the same SiO_2/Si substrates by chemical vapor deposition as described previously.[22,53] For the field effect devices, the electron beam lithography and evaporator were used to make the electrodes of Ni/Au (5 nm/80 nm) as source and drain contacts.[54] The back-gate voltage was applied between the p^{+2} Si substrate and the source/drain electrode.

The prepared 1L WS_2 samples were bonded to a printed circuit board (PCB) attached to a three-dimensional piezo-stage in a confocal micro-Raman/PL spectroscopic system with a liquid helium cryostat.[55] Gated PL measurements were conducted at room temperature (300 K) in vacuum (~1×10^{-5} mBar) and then at 4.2 K where the helium gas was filled into the vacuum tube to approach a pressure of 19 mbar before loading into the liquid-helium cryostat. An 532 nm Nd:YAG laser was used to excite the samples through a ×50 objective lens, and the PL signals were collected by a grating (600/mm) spectrometer with a thermoelectrically cooled detector. The laser spot size on samples is ~1 μm. The excitation power on samples was tunable in the range from 0 to10 mW. Electrical transport data were measured by a commercial Keithley 4200 parameter analyzer.

Conflict of Interest: The authors declare no competing financial interest.

Acknowledgment. This work is mainly supported by the Singapore National Research Foundation under NRF RF Award No. NRFRF2010-07, MOE Tier 2 MOE2012-T2-2-049, and A*Star SERC PSF grant 1321202101. Shang thanks Dr. Rui Chen, Dr. Tingchao He, and Ms. Lin Ma for helpful discussions.

Supporting Information Available: Supplementary figures (Figures S1−S8) and the corresponding discussion. This material is available free of charge *via* the Internet at http://pubs.acs.org.

REFERENCES AND NOTES

1. Wang, Q. H.; Kalantar-Zadeh, K.; Kis, A.; Coleman, J. N.; Strano, M. S. Electronics and Optoelectronics of Two-Dimensional Transition Metal Dichalcogenides. *Nat. Nanotechnol.* **2012**, *7*, 699–712.
2. Jariwala, D.; Sangwan, V. K.; Lauhon, L. J.; Marks, T. J.; Hersam, M. C. Emerging Device Applications for Semiconducting Two-Dimensional Transition Metal Dichalcogenides. *ACS Nano* **2014**, *8*, 1102–1120.
3. Xu, X. D.; Yao, W.; Xiao, D.; Heinz, T. F. Spin and Pseudospins in Layered Transition Metal Dichalcogenides. *Nat. Phys.* **2014**, *10*, 343–350.
4. Radisavljevic, B.; Radenovic, A.; Brivio, J.; Giacometti, V.; Kis, A. Single-Layer MoS_2 Transistors. *Nat. Nanotechnol.* **2011**, *6*, 147–150.
5. Lopez-Sanchez, O.; Lembke, D.; Kayci, M.; Radenovic, A.; Kis, A. Ultrasensitive Photodetectors Based on Monolayer MoS_2. *Nat. Nanotechnol.* **2013**, *8*, 497–501.
6. Ross, J. S.; Klement, P.; Jones, A. M.; Ghimire, N. J.; Yan, J. Q.; Mandrus, D. G.; Taniguchi, T.; Watanabe, K.; Kitamura, K.; Yao, W.; *et al.* Electrically Tunable Excitonic Light-Emitting Diodes Based on Monolayer WSe_2 p-n Junctions. *Nat. Nanotechnol.* **2014**, *9*, 268–272.

7. Sundaram, R. S.; Engel, M.; Lombardo, A.; Krupke, R.; Ferrari, A. C.; Avouris, P.; Steiner, M. Electroluminescence in Single Layer MoS_2. *Nano Lett.* **2013**, *13*, 1416–1421.
8. Jo, S.; Ubrig, N.; Berger, H.; Kuzmenko, A. B.; Morpurgo, A. F. Mono- and Bilayer WS_2 Light-Emitting Transistors. *Nano Lett.* **2014**, *14*, 2019–2025.
9. Mak, K. F.; He, K.; Lee, C.; Lee, G. H.; Hone, J.; Heinz, T. F.; Shan, J. Tightly Bound Trions in Monolayer MoS_2. *Nat. Mater.* **2013**, *12*, 207–211.
10. Berghäuser, G.; Malic, E. Analytical Approach to Excitonic Properties of MoS_2. *Phys. Rev. B* **2014**, *89*, 125309.
11. Berkelbach, T. C.; Hybertsen, M. S.; Reichman, D. R. Theory of Neutral and Charged Excitons in Monolayer Transition Metal Dichalcogenides. *Phys. Rev. B* **2013**, *88*, 045318.
12. Komsa, H.-P.; Krasheninnikov, A. V. Effects of Confinement and Environment on the Electronic Structure and Exciton Binding Energy of MoS_2 from First Principles. *Phys. Rev. B* **2012**, *86*, 241201.
13. Cheiwchanchamnangij, T.; Lambrecht, W. R. L. Quasiparticle Band Structure Calculation of Monolayer, Bilayer, and Bulk MoS_2. *Phys. Rev. B* **2012**, *85*, 205302.
14. Ramasubramaniam, A. Large Excitonic Effects in Monolayers of Molybdenum and Tungsten Dichalcogenides. *Phys. Rev. B* **2012**, *86*, 115409.
15. Qiu, D. Y.; da Jornada, F. H.; Louie, S. G. Optical Spectrum of MoS_2: Many-Body Effects and Diversity of Exciton States. *Phys. Rev. Lett.* **2013**, *111*, 216805.
16. Zhang, C.; Johnson, A.; Hsu, C. L.; Li, L. J.; Shih, C. K. Direct Imaging of Band Profile in Single Layer MoS_2 on Graphite: Quasiparticle Energy Gap, Metallic Edge States, and Edge Band Bending. *Nano Lett.* **2014**, *14*, 2443–2447.
17. Ugeda, M. M.; Bradley, A. J.; Shi, S.-F.; da Jornada, F. H.; Zhang, Y.; Qiu, D. Y.; Mo, S.-K.; Hussain, Z.; Shen, Z.-X.; Wang, F.; *et al.* Giant Bandgap Renormalization and Excitonic Effects in a Monolayer Transition Metal Dichalcogenide Semiconductor. *Nat. Mater.* **2014**, *13*, 1091–1095.
18. Wang, G.; Marie, X.; Gerber, I.; Amand, T.; Lagarde, D.; Bouet, L.; Vidal, M.; Balocchi, A.; Urbaszek, B. Non-Linear Optical Spectroscopy of Excited Exciton States for Efficient Valley Coherence Generation in WSe_2 Monolayers. **2014**, arXiv:Condense Matter/1404.0056v1. *arXiv.org e-Print archive*. http://arxiv.org/abs/1404.0056v1 (accessed Oct 08, 2014).
19. Chernikov, A.; Berkelbach, T. C.; Hill, H. M.; Rigosi, A.; Li, Y.; Aslan, O. B.; Reichman, D. R.; Hybertsen, M. S.; Heinz, T. F. Exciton Binding Energy and Nonhydrogenic Rydberg Series in Monolayer WS_2. *Phys. Rev. Lett.* **2014**, *113*, 076802.
20. Zhu, B.; Chen, X.; Cui, X. Exciton Binding Energy of Monolayer WS_2. **2014**, arXiv:Condense Matter/1403.5108v2. *arXiv.org e-Print archive*. http://arxiv.org/abs/1403.5108v2 (accessed Oct 08, 2014).
21. Ye, Z.; Cao, T.; O'Brien, K.; Zhu, H.; Yin, X.; Wang, Y.; Louie, S. G.; Zhang, X. Probing Excitonic Dark States in Single-Layer Tungsten Disulfide. *Nature.* **2014**, *513*, 214–218.
22. Peimyoo, N.; Shang, J. Z.; Cong, C. X.; Shen, X. N.; Wu, X. Y.; Yeow, E. K. L.; Yu, T. Nonblinking, Intense Two-Dimensional Light Emitter: Monolayer WS_2 Triangles. *ACS Nano* **2013**, *7*, 10985–10994.
23. Ross, J. S.; Wu, S. F.; Yu, H. Y.; Ghimire, N. J.; Jones, A. M.; Aivazian, G.; Yan, J. Q.; Mandrus, D. G.; Xiao, D.; Yao, W.; *et al.* Electrical Control of Neutral and Charged Excitons in a Monolayer Semiconductor. *Nature Commun.* **2013**, *4*, 1474.
24. Jones, A. M.; Yu, H. Y.; Ghimire, N. J.; Wu, S. F.; Aivazian, G.; Ross, J. S.; Zhao, B.; Yan, J. Q.; Mandrus, D. G.; Xiao, D.; *et al.* Optical Generation of Excitonic Valley Coherence in Monolayer WSe_2. *Nat. Nanotechnol.* **2013**, *8*, 634–638.
25. Mitioglu, A. A.; Plochocka, P.; Jadczak, J. N.; Escoffier, W.; Rikken, G. L. J. A.; Kulyuk, L.; Maude, D. K. Optical Manipulation of the Exciton Charge State in Single-Layer Tungsten Disulfide. *Phys. Rev. B* **2013**, *88*, 245403.
26. Mai, C.; Barrette, A.; Yu, Y. F.; Semenov, Y. G.; Kim, K. W.; Cao, L. Y.; Gundogdu, K. Many-Body Effects in Valleytronics: Direct Measurement of Valley Lifetimes in Single-Layer MoS_2. *Nano Lett.* **2014**, *14*, 202–206.
27. Ye, Y.; Ye, Z.; Gharghi, M.; Zhu, H.; Zhao, M.; Wang, Y.; Yin, X.; Zhang, X. Exciton-Dominant Electroluminescence from a Diode of Monolayer MoS_2. *Appl. Phys. Lett.* **2014**, *104*, 193508.
28. Zhang, C.; Wang, H.; Chan, W.; Manolatou, C.; Rana, F. Absorption of Light by Excitons and Trions in Monolayers of Metal Dichalcogenide MoS_2: Experiments and Theory. *Phys. Rev. B* **2014**, *89*, 205436.
29. Hawrylak, P. Optical Properties of a Two-Dimensional Electron Gas: Evolution of Spectra from Excitons to Fermi-Edge Singularities. *Phys. Rev. B* **1991**, *44*, 3821–3828.
30. Huard, V.; Cox, R. T.; Saminadayar, K.; Arnoult, A.; Tatarenko, S. Bound States in Optical Absorption of Semiconductor Quantum Wells Containing a Two-Dimensional Electron Gas. *Phys. Rev. Lett.* **2000**, *84*, 187–190.
31. Trankle, G.; Lach, E.; Forchel, A.; Scholz, F.; Ell, C.; Haug, H.; Weimann, G.; Griffiths, G.; Kroemer, H.; Subbanna, S. General Relation between Band-Gap Renormalization and Carrier Density in Two-Dimensional Electron-Hole Plasmas. *Phys. Rev. B* **1987**, *36*, 6712–6714.
32. Trankle, G.; Leier, H.; Forchel, A.; Haug, H.; Ell, C.; Weimann, G. Dimensionality Dependence of the Band-Gap Renormalization in Two-Dimensional and 3-Dimensional Electron-Hole Plasmas in GaAs. *Phys. Rev. Lett.* **1987**, *58*, 419–422.
33. Ju, L.; Velasco, J., Jr.; Huang, E.; Kahn, S.; Nosiglia, C.; Tsai, H. Z.; Yang, W.; Taniguchi, T.; Watanabe, K.; Zhang, Y.; *et al.* Photoinduced Doping in Heterostructures of Graphene and Boron Nitride. *Nat. Nanotechnol.* **2014**, *9*, 348–352.
34. Tiberj, A.; Rubio-Roy, M.; Paillet, M.; Huntzinger, J. R.; Landois, P.; Mikolasek, M.; Contreras, S.; Sauvajol, J. L.; Dujardin, E.; Zahab, A. A. Reversible Optical Doping of Graphene. *Sci. Rep.* **2013**, *3*, 2355.
35. Mak, K. F.; He, K.; Shan, J.; Heinz, T. F. Control of Valley Polarization in Monolayer MoS_2 by Optical Helicity. *Nat. Nanotechnol.* **2012**, *7*, 494–498.
36. Korn, T.; Heydrich, S.; Hirmer, M.; Schmutzler, J.; Schüller, C. Low-Temperature Photocarrier Dynamics in Monolayer MoS_2. *Appl. Phys. Lett.* **2011**, *99*, 102109.
37. Sercombe, D.; Schwarz, S.; Del Pozo-Zamudio, O.; Liu, F.; Robinson, B. J.; Chekhovich, E. A.; Tartakovskii, I. I.; Kolosov, O.; Tartakovskii, A. I. Optical Investigation of the Natural Electron Doping in Thin MoS_2 Films Deposited on Dielectric Substrates. *Sci. Rep.* **2013**, *3*, 3489.
38. Tongay, S.; Suh, J.; Ataca, C.; Fan, W.; Luce, A.; Kang, J. S.; Liu, J.; Ko, C.; Raghunathanan, R.; Zhou, J.; *et al.* Defects Activated Photoluminescence in Two-Dimensional Semiconductors: Interplay between Bound, Charged, and Free Excitons. *Sci. Rep.* **2013**, *3*, 2657.
39. Langbein, W.; Hvam, J. M. Dephasing in the Quasi-Two-Dimensional Exciton-Biexciton System. *Phys. Rev. B* **2000**, *61*, 1692–1695.
40. Feldmann, J.; Peter, G.; Gobel, E. O.; Dawson, P.; Moore, K.; Foxon, C.; Elliott, R. J. Linewidth Dependence of Radiative Exciton Lifetimes in Quantum-Wells. *Phys. Rev. Lett.* **1987**, *59*, 2337–2340.
41. Schultheis, L.; Honold, A.; Kuhl, J.; Kohler, K.; Tu, C. W. Optical Dephasing of Homogeneously Broadened Two-Dimensional Exciton-Transitions in GaAs Quantum-Wells. *Phys. Rev. B* **1986**, *34*, 9027–9030.
42. Kim, J. C.; Wake, D. R.; Wolfe, J. P. Thermodynamics of Biexcitons in a GaAs Quantum-Well. *Phys. Rev. B* **1994**, *50*, 15099–15107.
43. Kono, S.; Kirihara, A.; Tomita, A.; Nakamura, K.; Fujikata, J.; Ohashi, K.; Saito, H.; Nishi, K. Excitonic Molecule in a Quantum Dot: Photoluminescence Lifetime of a Single InAs/GaAs Quantum Dot. *Phys. Rev. B* **2005**, *72*, 155307.
44. Ghali, M.; Ohtani, K.; Ohno, Y.; Ohno, H. Generation and Control of Polarization-Entangled Photons from GaAs Island Quantum Dots by an Electric Field. *Nat. Commun.* **2012**, *3*, 661.
45. Abbarchi, M.; Mastrandrea, C. A.; Kuroda, T.; Mano, T.; Sakoda, K.; Koguchi, N.; Sanguinetti, S.; Vinattieri, A.; Gurioli, M. Exciton Fine Structure in Strain-Free GaAs/$Al_{0.3}Ga_{0.7}As$

Quantum Dots: Extrinsic effects. *Phys. Rev. B* **2008**, *78*, 125321.
46. Trotta, R.; Wildmann, J. S.; Zallo, E.; Schmidt, O. G.; Rastelli, A. Highly Entangled Photons from Hybrid Piezoelectric-Semiconductor Quantum Dot Devices. *Nano Lett.* **2014**, *14*, 3439–3444.
47. Akopian, N.; Lindner, N. H.; Poem, E.; Berlatzky, Y.; Avron, J.; Gershoni, D.; Gerardot, B. D.; Petroff, P. M. Entangled Photon Pairs from Semiconductor Quantum Dots. *Phys. Rev. Lett.* **2006**, *96*, 130501.
48. Shiau, S. Y.; Combescot, M.; Chang, Y. C. Electronic Structure and Absorption Spectrum of Biexciton Obtained by Using Exciton Basis. *Ann. Phys.* **2013**, *336*, 309–330.
49. Shi, H.; Pan, H.; Zhang, Y.-W.; Yakobson, B. I. Quasiparticle Band Structures and Optical Properties of Strained Monolayer MoS_2 and WS_2. *Phys. Rev. B* **2013**, *87*, 155304.
50. Sie, E. J.; Lee, Y.-H.; Frenzel, A. J.; Kong, J.; Gedik, N. Biexciton Formation in Monolayer MoS_2 Observed by Transient Absorption Spectroscopy. **2013**, arXiv:Condense Matter/1312.2918v1. *arXiv.org e-Print archive*. http://arxiv.org/abs/1312.2918v1 (accessed Oct 08, 2014).
51. Gong, C.; Colombo, L.; Wallace, R. M.; Cho, K. The Unusual Mechanism of Partial Fermi Level Pinning at Metal−MoS_2 Interfaces. *Nano Lett.* **2014**, *14*, 1714–1720.
52. Mai, C.; Semenov, Y. G.; Barrette, A.; Yu, Y.; Jin, Z.; Cao, L.; Kim, K. W.; Gundogdu, K. Exciton Valley Relaxation in a Single Layer of WS_2 Measured by Ultrafast Spectroscopy. *Phys. Rev. B* **2014**, *90*, 041414.
53. Cong, C. X.; Shang, J. Z.; Wu, X.; Cao, B. C.; Peimyoo, N.; Qiu, C.; Sun, L. T.; Yu, T. Synthesis and Optical Properties of Large-Area Single-Crystalline 2D Semiconductor WS_2 Monolayer from Chemical Vapor Deposition. *Adv. Opt. Mater.* **2014**, *2*, 131–136.
54. Peimyoo, N.; Li, J. W.; Shang, J. Z.; Shen, X. N.; Qiu, C. Y.; Xie, L. H.; Huang, W.; Yu, T. Photocontrolled Molecular Structural Transition and Doping in Graphene. *ACS Nano* **2012**, *6*, 8878–8886.
55. Qiu, C. Y.; Shen, X. N.; Cao, B. C.; Cong, C. X.; Saito, R.; Yu, J. J.; Dresselhaus, M. S.; Yu, T. Strong Magnetophonon Resonance Induced Triple G-mode Splitting in Graphene on Graphite Probed by Micromagneto Raman Spectroscopy. *Phys. Rev. B* **2013**, *88*, 165407.